

## 산화아연/황화아연 양자점 나노결정에서의 향상된 자외선 방출

김기은 · 김웅 · 성윤모<sup>†</sup>

고려대학교 신소재공학부

## Enhanced UV-Light Emission in ZnO/ZnS Quantum Dot Nanocrystals

Ki-Eun Kim, Woong Kim, Yun-Mo Sung<sup>†</sup>

Department of Materials Science & Engineering, Korea University, Seoul 136-713, South Korea

(2008년 10월 20일 접수 : 2008년 11월 20일 최종수정 : 2008년 11월 27일 채택)

**Abstract** ZnO/ZnS core/shell nanocrystals (~5-7 nm in diameter) with a size close to the quantum confinement regime were successfully synthesized using polyol and thermolysis. X-ray diffraction (XRD) and high-resolution transmission electron microscopy (HRTEM) analyses reveal that they exist in a highly crystalline wurtzite structure. The ZnO/ZnS nanocrystals show significantly enhanced UV-light emission (~384 nm) due to effective surface passivation of the ZnO core, whereas the emission of green light (~550 nm) was almost negligible. They also showed slight photoluminescence (PL) red-shift, which is possibly due to further growth of the ZnO core and/or the extension of the electron wave function to the shell. The ZnO/ZnS core/shell nanocrystals demonstrate strong potential for use as low-cost UV-light emitting devices.

**Keywords** ZnO/ZnS, ZnO, nanocrystals, photoluminescence, UV-emission

### 1. Introduction

Over the past several years, semiconductor colloid nanocrystals have attracted a great deal of attention due to their unique physical properties arising from the quantum confinement effect that occurs when a semiconductor shrinks down below a critical size, so called Bohr's radius.<sup>1,2)</sup> Most research on the nanocrystals has been carried out to acquire modulated band gap emission or improved luminescence efficiency of nanometer sized semiconductors for the optical, electronic, optoelectronic applications such as light emitting diodes (LED), laser diodes (LD), optical data storage devices, and sensors.<sup>3-7)</sup> ZnO, one of II-VI semiconductors, possesses a wide energy band-gap (3.44 eV) and large excitation binding energy (60 meV) and hence it has taken particular attention in the applications for high-efficiency white LED source and high-density LD data storage. It is a very useful material that can be used as a transparent electrode in solar cells, chemical sensors, and catalysts as well.<sup>8,9)</sup> So far, however, most of researches on ZnO have been concentrated on thin film and nanowire structures,

while the research on colloidal ZnO nanocrystals is relatively rare.<sup>10)</sup> This is most likely due to the lack of reliable synthetic methods to produce ZnO particles in quantum confinement regime. The ZnO-based nanocrystals may find applications for low-cost LED and LD devices when they are assembled in a two-dimensional film form. Also, it has strong potential to be used for fluorescent bioimaging or drug delivery due to their intrinsic nontoxicity which is one of the critical issues in biomedical applications of cadmium-bearing nanocrystals such as CdSe, CdS, and CdTe.<sup>11)</sup>

The luminescence is greatly affected in a nanostructure compared to in a bulk by diverse surface states arising from its higher surface to volume ratio. Modification of the surface of a nanomaterial by another one through the formation of a core/shell structure can greatly affect its luminescent property.<sup>12)</sup> There have been quite a number of reports on the core/shell structures, where coating of a higher band-gap shell material effectively enhanced the optical property of the core material.<sup>13-15)</sup> It has been shown that the radiative emission from quantum dot nanocrystals can also be enhanced by passivating surface dangling bonds.<sup>16)</sup>

ZnS is a II-VI semiconductor having a higher energy band-gap (3.67 eV) than ZnO and it also has the same

<sup>†</sup>Corresponding author

E-Mail : ymsung@korea.ac.kr(Y. M. Sung)

wurtzite structure with lattice parameters ( $a=3.81$ ,  $c=6.26$  Å) close to ZnO ( $a=3.25$ ,  $c=5.21$  Å), which allows ZnS to be used as a appropriate shell for the ZnO core. Recently, Li *et al.* reported the improved optical property from ZnO/ZnS core/shell nanowires formed by thermal vapor transport method.<sup>17)</sup> Zhu *et al.* introduced synthesis of ZnO/ZnS core/shell spheres ( $\sim 700$  nm) using partial chemical conversion of the surface of ZnO ( $\sim 400$  nm).<sup>18)</sup>

However, to date there is no report of successful synthesis of ZnO/ZnS core/shell nanocrystals that are close to Bohr radius in diameter ( $\sim 5$  nm). This is probably due to the possibility that aqueous environment can cause an unwanted chemical reaction such as hydroxide formation when moisture sensitive materials are synthesized.<sup>19)</sup> In this study, ZnO and ZnO/ZnS nanocrystals close to the Bohr's radius were successfully fabricated by polyol and thermolysis in a non-aqueous environment. The crystallinity and optical properties were investigated and compared to each other.

## 2. Experimental Procedure

The ZnO nanocrystals were prepared by modifying the procedure described by Kim *et al.*<sup>20)</sup>  $(\text{ZnCH}_3)_2$  were dissolved in isopropanol in a three-neck flask and heated at  $40^\circ\text{C}$  for 2 h under stirring. Next, trioctylphosphine (TOP) was added in the solution as a surfactant. Then this solution was heated at  $150^\circ\text{C}$  for 5 h under stirring. After heating, white suspension of ZnO nanocrystals was obtained. To overcoat the ZnO nanocrystals with ZnS, a mixed solution of  $(\text{ZnCH}_3)_2$  (0.133 g),  $(\text{TMS})_2\text{S}$  (0.138 g), and tri-butyl phosphate (TBP) (5.366 g) was slowly dropped into the flask containing ZnO nanoparticles at the rate of  $\sim 0.1$  ml/min. This solution was maintained at  $130^\circ\text{C}$  for 2 h. Methanol (20 ml) was added into the solution to precipitate particles and the particles were separated by centrifugation. The nanocrystals were redispersed in hexane (20 ml) and after repeating this process, ZnO/ZnS nanocrystals were obtained with very narrow size distribution ( $\sim 5$ -7 nm). The synthesis of ZnO nanoparticles is described in more detail as follows. The particles were synthesized using a non-hydrolytic method which is thermolysis of a single molecular precursor without oxygen source. By mixing  $(\text{ZnCH}_3)_2$  with isopropanol and heating for 2 h,  $\text{CH}_3\text{ZnO-i-Pr}$  was produced.<sup>21)</sup> After self-decomposition of  $\text{CH}_3\text{ZnO-i-Pr}$  with a capping agent, TOP, ZnO nanocrystals were fabricated and

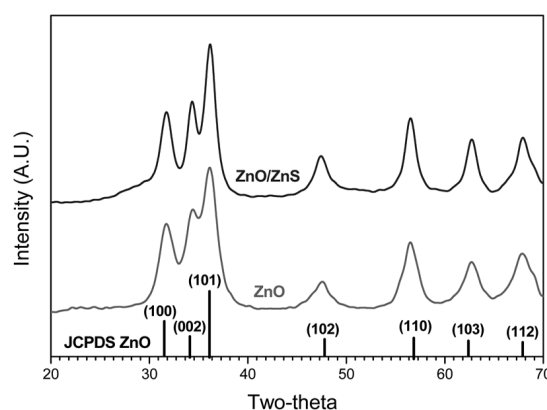


**Fig. 1.** X-ray diffraction (XRD) patterns of (a) ZnO and (b) ZnO/ZnS nanocrystals showing formation of wurtzite structure. JCPDS for ZnO is inserted for comparison.

gaseous methane ( $\text{CH}_4$ ) and propylene ( $\text{CH}_2\text{CHCH}_3$ ) were released. Self-decomposition of  $\text{CH}_3\text{ZnO-i-Pr}$  into ZnO and gaseous by-products can occur through the breakage of bonding. Synthesized ZnO nanocrystals were stabilized due to TOP which is known as a strong donor ligand, having both high polarity and polarizability contributing to its donor strength. TOP prevents agglomeration between particles and provide them with superior solubility in nonpolar solvents owing to its alkyl groups.<sup>22)</sup> ZnS molecules were formed at the surface of ZnO as a result of reaction between  $\text{Me}_2\text{Zn}$  and  $(\text{TMS})_2\text{S}$ . The core ZnO nanocrystals can serve as seeds for nucleation and growth of the ZnS shell.<sup>23)</sup>

## 3. Results and Discussion

Fig. 1 shows X-ray diffraction (XRD, Rigaku Ultima 2000,  $\lambda = 1.5418\text{\AA}$ ) patterns of ZnO and ZnO/ZnS nanostructures, respectively. The two patterns were almost identical and both the ZnO and ZnO/ZnS nanocrystals were identified to be of wurtzite structure with high crystallinity by comparing with the JCPDS card (#03-0891). However, the ZnO/ZnS core/shell nanostructures showed increased peak sharpness compared to the bare ZnO, which implies slightly increased size and crystallinity in ZnO/ZnS. One can use following Scherrer's formula for the size estimation of nanocrystals.

$$d = \frac{0.9\lambda}{FWHM \cdot \cos \theta_B} \quad (1)$$

where  $d$  is the size of crystals,  $\lambda$  is the wavelength of Cu  $K_\alpha$ , FWHM is the full width at half maximum of a

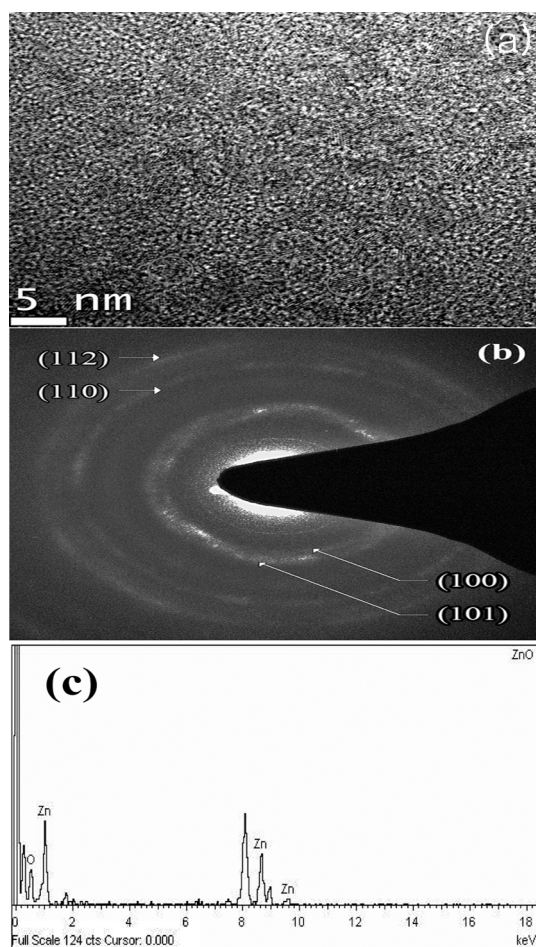


**Fig. 2.** High-resolution transmission electron microscopy (HRTEM) images (a), corresponding selected area electron diffraction (SAED) patterns (b), and EDS results (c) of ZnO nanocrystals.

diffraction peak, and  $\theta_b$  is the Bragg's angle for the diffraction. By considering (110) peak we obtained the averaged particle size of  $\sim 4.4$  and  $\sim 6.2$  nm for the bare and core/shell nanocrystals, respectively. The ZnS shell seems to be too thin to participate in the diffraction. XRD peak shift frequently found in core/shell structure did not occur due to the close lattice parameter values of ZnO and ZnS. High-resolution transmission electron microscopy (HRTEM, FEI Technai G2 F30, 300 kV) images of ZnO and ZnO/ZnS nanocrystals in Fig. 2 and 3 show that they are in a spherical shape with an average size of  $\sim 3$ -4 and  $\sim 5$ -7 nm, respectively, having narrow size distribution. This result is in good agreement with the size estimation using the Scherrer formula (Equation 1).

Size difference between the ZnO and ZnO/ZnS nanocrystal, in addition to the ZnS shell coating, could possibly be attributed to the further growth of ZnO core

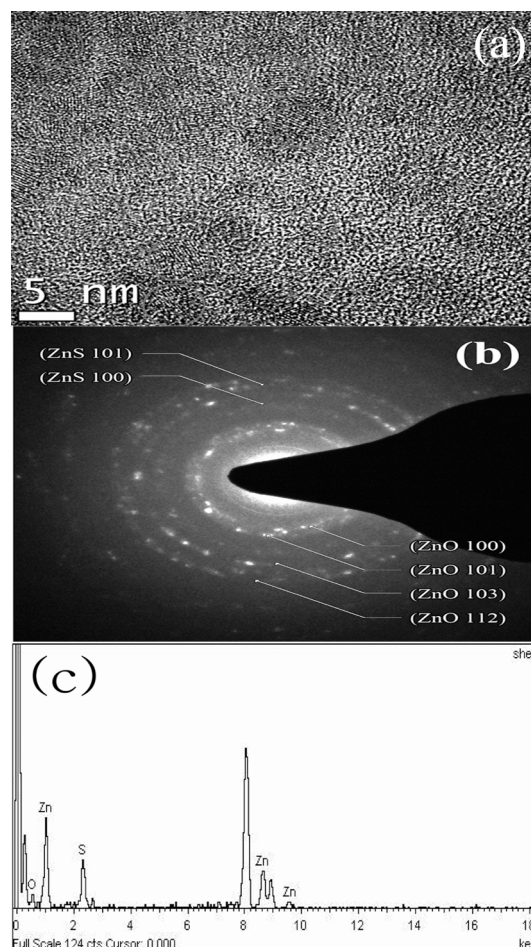


**Fig. 3.** High-resolution transmission electron microscopy (HRTEM) images (a), corresponding selected area electron diffraction (SAED) patterns (b), and EDS results (c) ZnO/ZnS nanocrystals.

during shell formation, which makes resulting shell thinner than 1 nm. The selected area electron diffraction (SAED) ring patterns clearly show the crystallinity of wurtzite ZnO for the bare ZnO nanocrystals as shown in Fig. 2 Also, the SAED pattern of the ZnO/ZnS samples in Fig. 3 shows two sets of rings each corresponding to wurtzite ZnO and ZnS, respectively. This is a clear evidence for the formation of ZnO/ZnS core/shell structure. The diffraction rings of ZnS, however, are much weaker than those of ZnO, which indicates that the ZnS shell could be very thin and/or the crystallinity may be not as high. The Energy dispersive x-ray spectroscopy (EDS: Oxford, Inca, Oxon, UK) spectrum for the ZnO/ZnS also reveals the presence of Zn, O, and S in the specimen, implying that the ZnS shell formation. It should be noted that ZnS phase could not be detected from ZnO/ZnS by XRD due to its relatively low

resolution compared to the HRTEM. The UV-visible absorption (JASCO UV-Visible Spectrophotometer: V530, Tokyo, Japan) spectra of ZnO and ZnO/ZnS are respectively presented in Fig. 4. Compared to peak position of ZnO, that of ZnO/ZnS shows slight red-shift. This probably means the overgrowth of core ZnO crystals during the shell formation for 2 h and the extension of electron wave function of ZnO core to the ZnS shell. Fig. 5 shows photoluminescence (PL: Hitachi F-4500, Tokyo, Japan) results of ZnO and ZnO/ZnS nanocrystals. Solutions with identical concentration of nanocrystals were used for the PL experiments. The PL spectra of ZnO are composed of two emission bands in the UV/visible range. UV emission at 376 nm is correlated with radiative recombination between conduction band electrons and valence band holes during relaxation. The UV-light emission at 376 nm is slightly blue shifted compared to bulk ZnO having theoretical energy band-gap of  $\sim 3.2$  eV showing UV-light emission at  $\sim 380$  nm. This blue shift implies that the quantum confinement effect takes place in the bare ZnO. Since the average diameter of the bare ZnO ( $d \sim 3$ – $4$  nm) is slightly smaller than two times its Bohr's radius, which is 2.34 nm, quantum confinement effect could be observed. The shift between the lowest energy peak in the absorption spectrum of a semiconductor nanocrystals and emission peak is called the Stokes shift.<sup>5)</sup> Because of the Stokes shift, the wavelength of UV absorption band-edge of nanocrystals is shorter than that of the UV-emission peak position. Also, a strong and broad green luminescence peak is observed in the range of 450–650 nm (peak at 550 nm). The green emission appearance in ZnO has been extensively studied by Vanheusden *et al.*<sup>24)</sup> They suggested that visible emission is owing to the recombination of electrons in singly occupied vacancies with holes in the valence band, and the green emission is related to trap site at the nanocrystal surface. Furthermore, Dijken *et al.*<sup>25)</sup> describe that it is due to the non-radiative recombination between deep-level holes trapped in oxygen vacancy centers ( $V_O^{\bullet\bullet}$ ) and shallow-level electrons. Thus, these oxygen vacancies are in general accepted to be responsible for the broad visible-range emission in ZnO. Quenching of the green emission has been extensively studied for example by Sekoguchi *et al.*<sup>26)</sup> Recently they reported that quenching of visible luminescence could be accompanied by the enhancement of the band edge UV luminescence by hydrogen plasma treatment to ZnO.

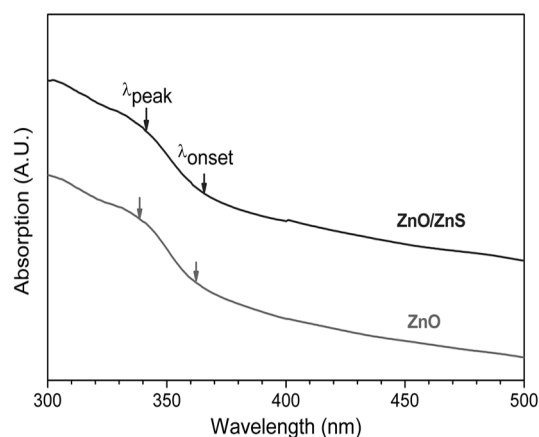


**Fig. 4.** UV-Visible absorption spectra of ZnO and ZnO/ZnS nanocrystals. Absorption onset and peak positions are indicated as arrows, respectively.

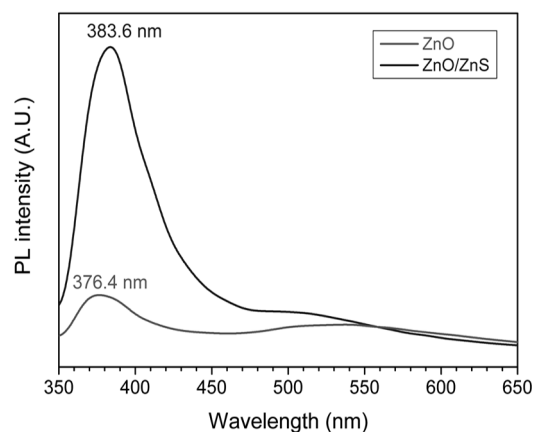


**Fig. 5.** Photoluminescence (PL) spectra of ZnO and ZnO/ZnS nanocrystals.

Similarity to the UV-visible absorption peaks, slight red shift was found in the PL peaks of the ZnO/ZnS core/shell nanocrystals compared to ZnO nanocrystals due to the overgrowth of ZnO core and the extension of electron wave function to the ZnS shell. The PL peak of ZnO/ZnS showed about seven times enhanced UV-emission intensity due to the effective surface passivation by the ZnS shell.  $Zn^{2+}$  and  $S^{2-}$  ions in the ZnS shell could combine with the surface ions of  $O^{2-}$  and  $Zn^{2+}$  in ZnO, respectively to effectively passivate the dangling bonds acting as strong trap sites for the electron and holes. Therefore, the removal of the surface dangling bonds by applying ZnS shell could enhance radiative recombination between electrons and holes to increase the PL intensity of the ZnO nanocrystals. Also, the non-radiative green emission was almost negligible in the ZnO/ZnS nanocrystals compared to radiative UV-light emission.

#### 4. Conclusions

In summary, ZnO/ZnS core/shell nanocrystals ( $d \sim 5$  nm) were successfully synthesized using nonhydrolytic polyol and thermolysis method. It was demonstrated that ZnO/ZnS nanocrystals can more controllably be synthesized in non-aqueous environment, leading to well defined nanocrystal structures that are just several nanometers in diameter. XRD and HRTEM analyses reveal that they are in highly crystalline wurtzite structure. ZnS shell formation on ZnO core was confirmed by SAED, EDS, and enhanced photoluminescence intensity. The quantum yield of ZnO nanocrystals were significantly enhanced owing to the effective passivation of trap sites of ZnO with ZnS. The ZnO/ZnS core/shell nanocrystals has strong potential to be applied to various areas such as low-cost photoelectronics, optical sensors, biosensors, etc.

#### Acknowledgements

This work was supported by the Korea-Israel Joint Research Fund Program of Korean Israeli Science Sharing (KISS) Program in 2007.

#### References

1. C. B. Murray, D. J. Norris and M. G. Bawendi, J. Am. Chem. Soc., **1158**, 8706, (1993).
2. V. L. Colvun, M. C. Schlamp and A. P. Alivisatos, Nature, **370**, 354, (1994).
3. Y. M. Sung, Y. J. Lee and K. S. Park, J. Am. Chem. Soc., **128**, 9003, (2006).
4. J. P. Hsu, Z. R. Tian, N. C. Simmons, C. M. Matzke, J. A. Voigt and J. Liu, Nano Lett., **5**, 83, (2005).
5. B. O. Dabbousi, J. Rodriguez-Viejo, F. V. Mikulec, J. R. Heine, H. Mattoussi, R. Ober, K. F. Jensen and M. G. Bawendi, J. Phys. Chem. B., **101**, 9463, (1997).
6. M. V. Artemyev, U. Woggon, R. Wannemacher, H. Jaschinski and W. Langbein, Nano Lett., **1**, 309, (2001).
7. W.-C. Kwak, T.-G. Kim, W.-S. Chae and Y.-M. Sung, Appl. Phys. Lett., **90**, 173111, (2007).
8. V. Noack, H. Weller and A. Eychmuller, J. Phys. Chem. B., **106**, 8514, (2002).
9. J. A. Rodriguez, T. Jirsak, J. Dvorak, S. Sambasivan and D. Fischer, J. Phys. Chem. B., **104**, 319, (2000).
10. M.-K. Lee, T.-G. Kim, W. Kim and Y.-M. Sung, J. Phys. Chem. C., **112**, 10079, (2008).
11. R. Bravner, R. Ferrari-Iliou, N. Brivois, S. Djediat, M. F. Benedetti, F. Fievet, Nano Lett., **6**, 866, (2006).
12. T. Gao, Q. H. Li and T. H. Wang, Chem. Mater., **17**, 887, (2005).
13. M. J. Murcia, D. L. Shaw, H. Woodruff, C. A. Naumann, B. A. Young and E. C. Long, Chem. Mater., **18**, 2219, (2006).
14. J. H. Song, T. Atay, S. Shi, H. Urabe and A. V. Nurmikko Nano Lett., **5**, 1557, (2005).
15. Y. Wang, Z. Tang, M. A. Correa-Duarte, L. M. Liz-Marzan and N. A. Kotov, J. Am. Chem. Soc., **125**, 2830, (2003).
16. Y. Ding, X. D. Wang and Z. L. Wang, Chem. Phys. Lett., **398**, 32, (2004).
17. J. Li, D. Zhao, X. Meng, Z. Zhang, J. Zhang, D. Shen, Y. Lu and X. Fan, J. Phys. Chem. B., **110**, 14685, (2006).
18. J. Geng, B. Liu, L. Xu, F. N. Hu and J. J. Zhu, Langmuir **23**, 10286, (2007).
19. S. Sapra and D. D. Sarma, Phys. Rev. B., **69**, 125304, (2004).
20. C. G. Kim, K. Sung, T. M. Chung, D. Y. Jung, and Y. Kim, Chem. Comm., **16**, 2068, (2003).
21. E. C. Ashby, G. F. Willard, A. B. Goel, J. Org. Chem., **44**, 1221, (1979).
22. O. Treu-Tler and R. J. Ahelrichs, Chem. Phys., **102**, 246, (1995).
23. M. Ethayaraja, C. Ravikumar, D. Muthkumaran, K. Dutta, R. Bandyopadhyaya, J. Phys. Chem. C., **111**, 3246, (2007).
24. K. Vanheusden, L. Warren, H. Seager, R. Tallant, A. Voigt and B. E. Gnade, J. Appl. Phys., **79**, 7983, (1996).
25. A. V. Dijken, E. A. Meulenkaamp, D. Vanmaekelbergh and A. Meijerink, J. Phys. Chem. B., **104**, 1715, (2000).
26. T. Sekiguchi, N. Ohashi and Y. Terada, J. Appl. Phys., **36**, L289, (1997).